Journal of Systems Engineering and Electronics
Vol. 33, No. 5, October 2022, pp.1 – 7

An effective array beamforming scheme based on branch-and-bound algorithm

YE Xiaodong, LI Li, WANG Hao, and TAO Shifei*

School of Electronic and Optical Engineering, Nanjing University of Science and Technology, Nanjing 210094, China

Abstract: In this paper, we propose an effective full array and sparse array adaptive beamforming scheme that can be applied for multiple desired signals based on the branch-and-bound algorithm. Adaptive beamforming for the multiple desired signals is realized by the improved Capon method. At the same time, the sidelobe constraint is added to reduce the sidelobe level. To reduce the pointing errors of multiple desired signals, the array response phase of the desired signal is firstly optimized by using auxilary variables while keeping the response amplitude unchanged. The whole design is formulated as a convex optimization problem solved by the branch-and-bound algorithm. In addition, the beamformer weight vector is penalized with the modified reweighted l_1-norm to achieve sparsity. Theoretical analysis and simulation results show that the proposed algorithm has lower sidelobe level, higher SINR, and less pointing error than the state-of-the-art methods in the case of a single expected signal and multiple desired signals.

Keywords: multiple desired signal, auxiliary variable, branch-and-bound algorithm, reweighted l_1-norm.

DOI: 10.23919/JSEE.2022.000123

1. Introduction

Adaptive array processing has become a vital part of modern electronic system design as it can easily control the beam, enhance the expected signal and effectively suppress spatial interference and noise [1−6]. The Capon algorithm based on the maximum output signal to interference-noise ratio (SINR) criterion has been rapidly developed and studied in the field of adaptive beamforming due to its advantages of ensuring high resolution in the case of few array elements and low snapshots [7−16]. In [10−14], the Capon algorithm for the full array was carried out, which was transformed into a convex relaxation problem. One proposed low-rank solution of the convex relaxation problem is eigenvalue decomposition [13−14], but the rank of the solution is not 1. If the rank is greater than 1, the solution is not feasible for the original synthesis problem [13]. In [15,16], the direct iterative rank refinement (DIRR) algorithm was used to solve the convex optimization problem iteratively, the rank of the obtained solution was close to 1, and the sidelobe level (SLL) was reduced by fixing the array output power. Nevertheless, there are amplitude and pointing errors for multiple expected signals, and the SLL is high.

In the field of sparse array beamforming [17−23], the reweighted l_1-norm is used to achieve sparseness and realize the maximization of SINR in the complex domain [20,21]. However, the challenges of pointing accuracy and SLL still exist. Although high SLL is suppressed using the linear fractional semidefinite relaxation (LFSDR) method in the real domain [23], the multi-expected signal pointing deviation has not been solved. Therefore, we need an algorithm to realize low SLL and accurate pointing for multiple desired signals.

In this paper, an effective array adaptive beamforming scheme is proposed based on the branch-and-bound algorithm for both single and multi-expected signals. The proposed scheme can achieve low SLL, high gain, deep nulling, and high pointing accuracy. The sidelobe constraint is added to the classical Capon algorithm based on the maximum SINR criterion to achieve excellent beamforming performance. Meanwhile, in order to improve the pointing accuracy of multiple desired signals, some variables are employed to optimize the array response phases. The solving process can be represented as a convex optimization problem by using the branch-and-bound method [24−26]. Furthermore, the modified reweighted l_1-norm is used to complete the sparsity. Numerical simulation examples are given to demonstrate the proposed algorithm.

This paper is organized as follows: Section 2 formulates the optimum array model based on maximizing the output SINR and solves the model by the branch-and-bound algorithm. Numerical simulation examples are listed in Section 3 and the conclusion follows in Section 4.

Manuscript received October 22, 2021.
*Corresponding author.
This work was supported by the National Key Research and Development Program (2021YFB3502500).

2. Methodology

2.1 Problem formulation

Given a uniform linear array with N sensors, for Q expected signals and P narrowband interferences whose arrival angles are $\theta_{s_q}(q=1,2,\cdots,Q)$ and $\theta_{i_p}(p=1,2,\cdots,P)$, the steering vectors are respectively

$$\begin{cases} \boldsymbol{a}(\theta_{s_q})=\left[1,\mathrm{e}^{\mathrm{j}\frac{2\pi}{\lambda}d\sin\theta_{sq}},\cdots,\mathrm{e}^{\mathrm{j}\frac{2\pi}{\lambda}(N-1)d\sin\theta_{sq}}\right]^{\mathrm{T}} \\ \boldsymbol{a}(\theta_{i_p})=\left[1,\mathrm{e}^{\mathrm{j}\frac{2\pi}{\lambda}d\sin\theta_{ip}},\cdots,\mathrm{e}^{\mathrm{j}\frac{2\pi}{\lambda}(N-1)d\sin\theta_{ip}}\right]^{\mathrm{T}} \end{cases} \tag{1}$$

where λ is the wavelength, and d is the interval spacing. The radiation pattern and normalized gain of the array can be written as

$$F(\theta)=\boldsymbol{w}^{\mathrm{H}}\boldsymbol{a}(\theta), \tag{2}$$

$$G(\theta)=\frac{|F(\theta)|^2}{\max|F(\theta)|^2}=\frac{\boldsymbol{w}^{\mathrm{H}}\boldsymbol{a}(\theta)\boldsymbol{a}(\theta)^{\mathrm{H}}\boldsymbol{w}}{\max[\boldsymbol{w}^{\mathrm{H}}\boldsymbol{a}(\theta)\boldsymbol{a}(\theta)^{\mathrm{H}}\boldsymbol{w}]}, \tag{3}$$

where $\boldsymbol{w}=[w_1,w_2,\cdots,w_N]^{\mathrm{T}}$ is the weight vector. The output SINR is

$$\mathrm{SINR}=\frac{\boldsymbol{w}^{\mathrm{H}}\boldsymbol{R}_s\boldsymbol{w}}{\boldsymbol{w}^{\mathrm{H}}\boldsymbol{R}_{i+n}\boldsymbol{w}} \tag{4}$$

where $\boldsymbol{R}_s=\sum_{q=1}^{Q}\sigma_{s_q}^2\boldsymbol{a}(\boldsymbol{\theta}_{s_q})\boldsymbol{a}(\boldsymbol{\theta}_{s_q})^{\mathrm{H}}$ is the covariance matrix of the expected signal. $\boldsymbol{R}_{i+n}=\sum_{p=1}^{P}\sigma_{i_p}^2\boldsymbol{a}(\theta_{i_p})\boldsymbol{a}(\theta_{i_p})^{\mathrm{H}}+\sigma_n^2\boldsymbol{I}_{N\times N}$ is the interference-plus-noise covariance matrix. $\sigma_{s_q}^2$ is the power of the expected signal. $\sigma_{i_p}^2$ and σ_n^2 are the interference and noise power, respectively, and $\boldsymbol{I}_{N\times N}$ is an $N\times N$ identity matrix. The maximum output SINR can be expressed as

$$\min_{\boldsymbol{w}}[\boldsymbol{w}^{\mathrm{H}}\boldsymbol{R}_{i+n}\boldsymbol{w}],\quad \text{s.t. } \boldsymbol{w}^{\mathrm{H}}\boldsymbol{R}_{s_q}\boldsymbol{w}=1. \tag{5}$$

2.2 Optimum array design

By uniformly sampling the sidelobe region, the angles and array manifold are θ_{l_h} and $\boldsymbol{a}(\theta_{l_h})(h=1,2,\cdots,H_s)$, where H_s is the sampling number of the sidelobe region. The corresponding gain can be described as

$$G(\boldsymbol{\theta}_{l_h})=\frac{\left|F(\boldsymbol{\theta}_{l_h})\right|^2}{\max|F|^2}=\frac{\boldsymbol{w}^{\mathrm{H}}\boldsymbol{a}(\theta_{l_h})\boldsymbol{a}(\theta_{l_h})^{\mathrm{H}}\boldsymbol{w}}{\max[\boldsymbol{w}^{\mathrm{H}}\boldsymbol{a}(\theta_{s_q})\boldsymbol{a}(\theta_{s_q})^{\mathrm{H}}\boldsymbol{w}]}=$$
$$\frac{\boldsymbol{w}^{\mathrm{H}}\boldsymbol{a}(\theta_{l_h})\boldsymbol{a}(\theta_{l_h})^{\mathrm{H}}\boldsymbol{w}}{\left|\boldsymbol{w}^{\mathrm{H}}\boldsymbol{a}(\theta_{s_q})\right|^2}. \tag{6}$$

In order to obtain the array pattern with the expected SLL of δ, the maximum output SINR with sidelobe constraints is

$$\min_{\boldsymbol{w}}[\boldsymbol{w}^{\mathrm{H}}R_{i+n}\boldsymbol{w}]$$
$$\text{s.t.}\begin{cases}\boldsymbol{w}^{\mathrm{H}}R_{s_q}\boldsymbol{w}=1\\ G(\theta_{l_h})\leqslant\delta\end{cases}. \tag{7}$$

Since $\boldsymbol{w}^{\mathrm{H}}\boldsymbol{R}_{s_q}\boldsymbol{w}$ satisfies

$$\boldsymbol{w}^{\mathrm{H}}\boldsymbol{R}_{s_q}\boldsymbol{w}=\sigma_{s_q}^2(\boldsymbol{w}^{\mathrm{H}}\boldsymbol{a}(\theta_{s_q}))(\boldsymbol{w}^{\mathrm{H}}\boldsymbol{a}(\boldsymbol{\theta}_{s_q}))^{\mathrm{H}}=$$
$$\sigma_{s_q}^2\left|\boldsymbol{w}^{\mathrm{H}}\boldsymbol{a}(\theta_{s_q})\right|^2, \tag{8}$$

we can derive

$$\min_{\boldsymbol{w}}[\boldsymbol{w}^{\mathrm{H}}R_{i+n}\boldsymbol{w}]$$
$$\text{s.t.}\begin{cases}\left|\boldsymbol{w}^{\mathrm{H}}\boldsymbol{a}(\theta_{s_q})\right|=\dfrac{1}{\sqrt{\sigma_{s_q}^2}}\\ \boldsymbol{w}^{\mathrm{H}}\boldsymbol{a}(\theta_{l_h})\boldsymbol{a}(\theta_{l_h})^{\mathrm{H}}\boldsymbol{w}\leqslant\delta\cdot\dfrac{1}{\sigma_{s_q}^2}\end{cases}. \tag{9}$$

By introducing new auxiliary variables $v_q(q=1,2,\cdots,Q)$, (9) can be equivalent to

$$\min_{\boldsymbol{w},v}[\boldsymbol{w}^{\mathrm{H}}R_{i+n}\boldsymbol{w}]$$
$$\text{s.t.}\begin{cases}\boldsymbol{w}^{\mathrm{H}}\boldsymbol{a}(\theta_{s_q})=v_q\\ \left|v_q\right|=\dfrac{1}{\sqrt{\sigma_{s_q}^2}}\\ \arg v_q\in\boldsymbol{\Theta}_q\\ \boldsymbol{w}^{\mathrm{H}}\boldsymbol{a}(\theta_{l_h})\boldsymbol{a}(\theta_{l_h})^{\mathrm{H}}\boldsymbol{w}\leqslant\delta\cdot\dfrac{1}{\sigma_{s_q}^2}\end{cases}. \tag{10}$$

Here $\boldsymbol{\Theta}_q$ is the set for the phase of auxiliary variables. When the real and imaginary parts of $\boldsymbol{\Theta}_q$ are separated, (10) can be expressed as

$$\min_{\substack{\Re(\boldsymbol{w}),\Im(\boldsymbol{w}),\\ \Re(\boldsymbol{v}),\Im(\boldsymbol{v})}}\{[\Re(\boldsymbol{w});\Im(\boldsymbol{w})]^{\mathrm{T}}\cdot\tilde{R}_{i+n}\cdot[\Re(\boldsymbol{w});\Im(\boldsymbol{w})]\}$$
$$\text{s.t.}\begin{cases}(\Re(\boldsymbol{w})+\mathrm{j}\Im(\boldsymbol{w}))^{\mathrm{H}}\boldsymbol{a}(\theta_{s_q})=\Re(v_q)+\mathrm{j}\cdot\Im(v_q) & \text{(11a)}\\ \sqrt{\Re(v_q)^2+\Im(v_q)^2}=\dfrac{1}{\sqrt{\sigma_{s_q}^2}} & \text{(11b)}\\ \arg(\Re(v_q)+\mathrm{j}\cdot\Im(v_q))\in\boldsymbol{\Theta}_q & \text{(11c)}\\ [\Re(\boldsymbol{w});\Im(\boldsymbol{w})]^{\mathrm{T}}\cdot\tilde{\boldsymbol{A}}_{l_h}\cdot[\Re(\boldsymbol{w});\Im(\boldsymbol{w})]\leqslant\delta\cdot\dfrac{1}{\sigma_{s_q}^2} & \text{(11d)}\end{cases}$$

where $\Re(\cdot)$ and $\Im(\cdot)$ represent the real and imaginary parts of parameters respectively. $\tilde{\boldsymbol{R}}_{i+n}$, $\boldsymbol{A}_{l_h}$, and $\tilde{\boldsymbol{A}}_{l_h}$ are

$$\begin{cases}\boldsymbol{A}_{l_h}\triangleq\boldsymbol{a}(\theta_{l_h})\boldsymbol{a}(\theta_{l_h})^{\mathrm{H}}\in\mathbf{C}^{\mathbf{N}\times\mathbf{N}},\ h=1,2,\cdots,H_s\\ \tilde{\boldsymbol{R}}_{i+n}=\begin{bmatrix}\Re(\boldsymbol{R}_{i+n}) & -\Im(\boldsymbol{R}_{i+n})\\ \Im(\boldsymbol{R}_{i+n}) & \Re(\boldsymbol{R}_{i+n})\end{bmatrix}\in\mathbf{R}^{2N\times2N}\\ \tilde{\boldsymbol{A}}_{ln}=\begin{bmatrix}\Re(\boldsymbol{A}_{ln}) & -\Im(\boldsymbol{A}_{l_h})\\ \Im(\boldsymbol{A}_{ln}) & \Re(\boldsymbol{A}_{l_h})\end{bmatrix}\in\mathbf{R}^{2N\times2N}\end{cases}, \tag{12}$$

Θ_q is assumed as $\left[\underline{\theta_q}, \overline{\theta_q}\right]$ with $\overline{\theta_q} - \underline{\theta_g} < 2\pi$, whose convex envelope $\mathrm{conv}(\Theta_q)$ of nonconvex constraints (11b) and (11c) can be defined [24] as

$$\mathrm{conv}(\Theta_q) = \left\{ [\Re(v_q), \Im(v_q)] \left| \sqrt{\Re(v_q)^2 + \Im(v_q)^2} \leqslant \frac{1}{\sqrt{\sigma_{s_q}^2}}, \right. \right.$$
$$\left. \left. \alpha_q \cdot \Re(v_q) + \beta_q \cdot \Im(v_q) - \gamma_q \cdot \frac{1}{\sqrt{\sigma_{s_q}^2}} \geqslant 0 \right\} \right. \tag{13}$$

where

$$\alpha_q = \cos\frac{\underline{\theta_q}, \overline{\theta_q}}{2},$$
$$\beta_q = \sin\frac{\underline{\theta_q}, \overline{\theta_q}}{2},$$
$$\gamma_q = \cos\frac{\underline{\theta_q}, \overline{\theta_q}}{2}.$$

Nonconvex equation (11) is rewritten as

$$\min_{\substack{\Re(\boldsymbol{w}),\Im(\boldsymbol{w}),\\ \Re(\boldsymbol{v}),\Im(\boldsymbol{v})}} \{[\Re(\boldsymbol{w}); \Im(\boldsymbol{w})]^{\mathrm{T}} \cdot \tilde{R}_{i+n} \cdot [\Re(\boldsymbol{w}); \Im(\boldsymbol{w})]\}$$
$$\text{s.t.} \begin{cases} (\Re(\boldsymbol{w}) + \mathrm{j} \cdot \Im(\boldsymbol{w}))^{\mathrm{H}} a(\theta_{s_q}) = \Re(v_q) + \mathrm{j} \cdot \Im(v_q) \\ [\Re(v_q), \Im(v_q)] \in \mathrm{conv}(\Theta_q) \\ [\Re(\boldsymbol{w}); \Im(\boldsymbol{w})]^{\mathrm{T}} \cdot \tilde{A}_{l_h} \cdot [\Re(\boldsymbol{w}); \Im(\boldsymbol{w})] \leqslant \delta \cdot \dfrac{1}{\sigma_{s_q}^2} \end{cases}. \tag{14}$$

Reweighted l_1-norm is introduced to promote sparsity, and the sparse array beamforming is expressed as

$$\min_{\substack{\Re(\boldsymbol{w}),\Im(\boldsymbol{w}),\\ \Re(\boldsymbol{v}),\Im(\boldsymbol{v})}} \left\{ [\Re(\boldsymbol{w}); \Im(\boldsymbol{w})]^{\mathrm{T}} \cdot \tilde{R}_{i+n} \cdot [\Re(\boldsymbol{w}); \Im(\boldsymbol{w})] + \right.$$
$$\left. \mu \cdot \sum_{i=1}^{N} (z \circ \left| \Re(\boldsymbol{w}) + \mathrm{j} \cdot \Im(\boldsymbol{w}) \right|) \right\}$$
$$\text{s.t.} \begin{cases} (\Re(\boldsymbol{w}) + \mathrm{j} \cdot \Im(\boldsymbol{w}))^{\mathrm{H}} \boldsymbol{a}(\theta_{s_q}) = \Re(v_q) + \mathrm{j} \cdot \Im(v_q) \\ [\Re(v_q), \Im(v_q)] \in \mathrm{conv}(\Theta_q) \\ [\Re(\boldsymbol{w}); \Im(w\boldsymbol{w})]^{\mathrm{T}} \cdot \tilde{A}_{l_h} \cdot [\Re(\boldsymbol{w}); \Im(\boldsymbol{w})] \leqslant \delta \cdot \dfrac{1}{\sigma_{s_q}^2} \end{cases} \tag{15}$$

where "$\circ$" is the element-wise product, μ is the coefficient to control the sparse rate, and z is the regularized weight vector. The expression of z can be written as

$$z = \frac{1}{\left|\Re(\boldsymbol{w}) + j \cdot \Im(\boldsymbol{w})\right| + \xi} \in \mathbf{R}^{N \times 1} \tag{16}$$

where ξ is a small number introduced to avoid dividing by zero. The branch-and-bound algorithm is used to solve (15), and the algorithm flow is shown in Algorithm 1.

Algorithm 1 Branch-and-bound algorithm for solving sparse array beamforming

Input: the example of (15), a sparse coefficient μ, a small number ξ, the number of iteration Niter, the expected number of excited elements Num, an error bound ε and the initial angular set $\Theta^1 = \Theta_1^1 \cup \Theta_2^1 \cup \cdots \cup \Theta_Q^1$.

1: **Loop**

2: Set $K = 1$, initialize z as the $N \times 1$ all-one matrix $\boldsymbol{I}_N$, iteratively solve (15), obtain the optimal solution $\boldsymbol{v}^1$ and the minimum value of objective function L^1, and generate the feasible solution where $\hat{\boldsymbol{v}}^1 = \mathrm{Map}(\boldsymbol{v}^1) = 1 \Big/ \sqrt{\sigma_{s_q}^2} \mathrm{e}^{\mathrm{j} \cdot \mathrm{phase}(\boldsymbol{v}^1)}$, substitute $\hat{\boldsymbol{v}}^1$ and $z = \boldsymbol{I}_N$ into (15) that has removed the convex envelope constraints, obtain $U = (\boldsymbol{w}^1)^{\mathrm{H}} \boldsymbol{R}_{i+n} \boldsymbol{w}^1$ and $\boldsymbol{w}^1$.

3: Construct an active node D, add $\{\Theta^1, \boldsymbol{v}^1, \hat{\boldsymbol{v}}^1, L^1, \boldsymbol{w}^1\}$ into node D.

4: **While** ($K \leqslant \mathrm{N_{iter}}$)

5: Select the active node $\{\Theta^K, \boldsymbol{v}^K, \hat{\boldsymbol{v}}^K, L^K, \boldsymbol{w}^K\}$ from D, where L^K is the smallest one of the kth nodes in D, then delete the selected node from D.

6: **If** $U - L^K < \varepsilon$, **then**
return $\hat{\boldsymbol{v}}^K$ and $\boldsymbol{w}^K$, go to Step 16.
End if

7: Renew $K = K + 1$.

8: Set q^* as the spoke-angle segmentation point on a unit circle, and calculate $q^* = \arg \min_{q \in \{1,2,\cdots,Q\}} \left| v_q^K \right|$, the equality $\Theta_{q^*}^K$ is divided into two subintervals $\Theta_{q^*-}^K$ and $\Theta_{q^*+}^K$ by using the spoke-angle splitting strategy, obtain the subsets $\Theta_-^K = \Theta_1^K \cup \Theta_2^K \cup \cdots \cup \Theta_{q^*-}^K \cup \cdots \cup \Theta_Q^K$ and $\Theta_+^K = \Theta_1^K \cup \Theta_2^K \cup \cdots \cup \Theta_{q^*+}^K \cup \cdots \cup \Theta_Q^K$.

9: Initialize $z = \boldsymbol{I}_N$ and iteratively solve (15) (Θ_-^K), obtain the optimal solution $\boldsymbol{v}_-^K$ and the minimum value of objective function L_-^K, and generate the feasible solution $\hat{\boldsymbol{v}}_-^K = \mathrm{Map}(\boldsymbol{v}_-^K) = 1/\sqrt{\sigma_{s_k}^2} \mathrm{e}^{\mathrm{j} \cdot \mathrm{phase}(\boldsymbol{v}_-^K)}$, substitute $\hat{\boldsymbol{v}}_-^K$ and $z = \boldsymbol{I}_N$ into (15) that has removed the convex envelope constraints, and obtain U_-^K and $\boldsymbol{w}_-^K$.

10: **If** $U > U_-^K$, **then** return $U = U_-^K$.

11: **If** $U > L_-^K$, **then**
add $\{\Theta_-^K, \boldsymbol{v}_-^K, \hat{\boldsymbol{v}}_-^K, L_-^K, \boldsymbol{w}_-^K\}$ into the node D.
End if

12: Similar to Step 9, iteratively solve (15) (Θ_+^K), and obtain $\boldsymbol{v}_+^K$, L_+^K, $\hat{\boldsymbol{v}}_+^K$, U_+^K, and $\boldsymbol{w}_+^K$.

13: **If** $U > U_+^K$, **then** return $U = U_+^K$.

14: **If** $U > L_+^K$, **then**
add $\{\Theta_+^K, \boldsymbol{v}_+^K, \hat{\boldsymbol{v}}_+^K, L_+^K, \boldsymbol{w}_+^K\}$ into node D.
End if

15: **End while**

16: **If** the number of excited array elements == Num the optimal value of the problem $\boldsymbol{w}^* = \boldsymbol{w}^K$, terminate the

algorithm.

else

update μ and ξ.

End if

17: **End loop**

The nonconvex constraint on (11) is relaxed to a convex constraint, which are decomposed into two disjoint subproblems according to the spoke-angle splitting strategy in each subsequent iteration process. In Step 2, the feasible solution to (11) is obtained by mapping the optimal solution to the subproblem; thereby, the lower bound of the subproblem and the upper bound of (11) are determined. When the lower bound is greater than the upper bound, a large number of redundant subproblems will be unprocessed and deleted. When the difference between the upper and lower bounds is slight or K reaches the specified maximum number of iterations, the optimal solution that satisfies the nonconvex constraint on (11) can be obtained. Therefore, the branch operation and the upper and lower bounds in the proposed algorithm can improve the problem's computational efficiency.

3. Numerical examples

In this section, several examples are provided to demonstrate the effectiveness of the proposed algorithm. Although Algorithm 1 is aimed at sparse array beamforming, the simulation results of the full array can still be obtained by removing the sparse steps involved in Algorithm 1. The sampling interval of the sidelobe region is $\lambda/(3(N-1)d)$.

3.1 Beamforming for the full array

Considering the optimization of a 16-element uniform linear array with $d=\lambda/2$, the signal to noise ratio (SNR) 0 dB and the interference to noise ratio (INR) 20 dB [16], the simulation results obtained by DIRR are given as a comparison. That is because DIRR has the characteristics of high positioning accuracy, fast convergence, high gain for the desired signal and deep nulling for the interference signals [16].

Firstly, assuming that there is only one signal of interest (SOI) and two interferers, the SOI impinges from $\theta_s=0°$, the arrival angles of interferers are $\theta_{i_1}=-30°$ and $\theta_{i_2}=14°$. The full array's normalized beam patterns for a single expected signal obtained by DIRR and the proposed results are plotted in Fig. 1, in which the proposed method performs lower SLL and higher SINR. There are 4.04 dB of SLL difference and 0.98 dB of output SINR difference between the proposed algorithm and the DIRR algorithm.

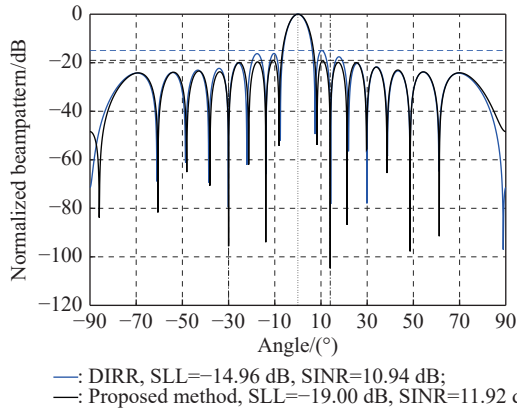

Fig. 1 Comparison of beam patterns simulated with two algorithms for a single expected signal

Secondly, for the case of multiple expected signals, it is assumed that there are three expected signals and two interference signals. The directions of SOI are $\theta_{s_1}=-19°$, $\theta_{s_2}=0°$, and $\theta_{s_3}=44°$, while $\theta_{i_1}=-49.6°$ and $\theta_{i_2}=22°$ are the interference directions. It can be seen from Fig. 2 that when δ is −10 dB, the SLL of the proposed algorithm achieves −9.59 dB and the SINR is 12.21 dB. When δ is −20 dB, the SLL achieves −18.94 dB, which is 13.39 dB lower than the DIRR algorithm, and the SINR is 11.76 dB with 0.38 dB higher. Moreover, in the case of multiple expected signals, the proposed algorithm has higher beam pointing accuracy, and the specific results are shown in Table 1.

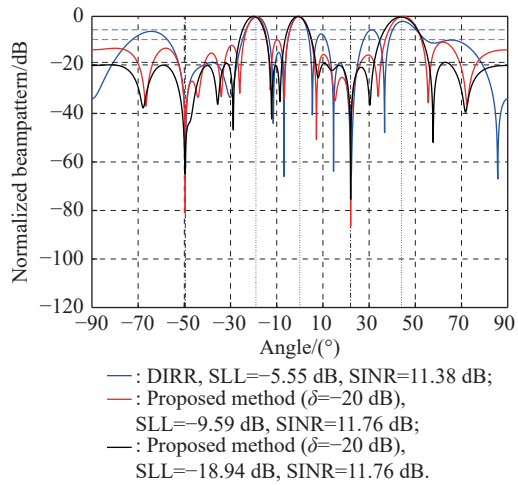

Fig. 2 Comparison of beam patterns simulated with two algorithms for multiple desired signals

Table 1 Comparison for the level of multiple expected signals with the DIRR and the proposed method

dB

Method		The level of desired signal			Average error
		$\theta_{s_1}=-19°$	$\theta_{s_2}=0°$	$\theta_{s_3}=44°$	
DIRR		−0.23	−0.09	−2.07	−0.80
Proposed method	$\delta=-10$ dB	−0.07	−0.07	−0.07	−0.07
	$\delta=-20$ dB	−0.24	−0.24	−0.24	−0.24

3.2 Beamforming for the sparse array

First of all, we consider the example in [23] that 14 elements of 20 uniformly-spaced elements with $d=\lambda/2$ are excited. Supposing that there is a single expected signal with SNR of 0 dB and three interference signals with each INR of 20 dB, the SOI angle is located at $\theta_s=10°$; the interference directions are $\theta_{i_1}=-40°$, $\theta_{i_2}=-20°$, and $\theta_{i_3}=50°$. The proposed algorithm has an SLL constraint of −20 dB. The array configurations obtained by results in [23] and the proposed method are shown in Fig. 3. The sparse array's normalized beam patterns obtained by the method in [23] and the proposed algorithm are compared in Fig. 4. We can find that the SLL obtained by the proposed algorithm is 7.62 dB lower, and the output SINR is 0.35 dB higher than the results in [23].

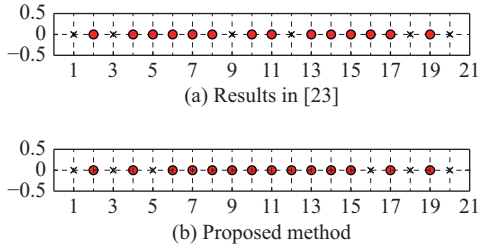

Fig. 3 Array configurations (*N*=20)

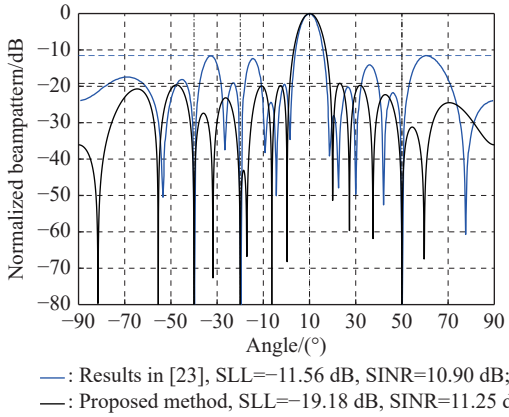

Fig. 4 Comparison of beam patterns simulated with the method in [23] and the proposed method for a single expected signal

Next, the example of the 16-element linear array in [21] with the sparse rate 50% is invested. Three desired signals impinge from $\theta_{s_1}=-50°$, $\theta_{s_2}=-25°$, $\theta_{s_3}=35°$, and three interference signals operate at $\theta_{i_1}=-40°$, $\theta_{i_2}=-30°$, and $\theta_{i_3}=30°$ incident simultaneously. The SNR is set as 0 dB, and the INR of each interferer is 30 dB. The simulation results of multiple point sources in [21] are used as a reference to assess the proposed method. Fig. 6 indicates that the output SINR of the proposed algorithm is 0.14 dB lower than the results in [21], but the SLL is 0.41 dB lower. Also, the average pointing error of the proposed algorithm for multiple desired signals is less, as shown in Table 2.

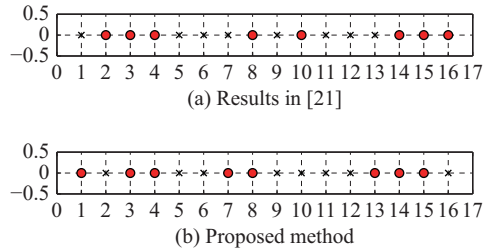

Fig. 5 Array configurations (*N*=16)

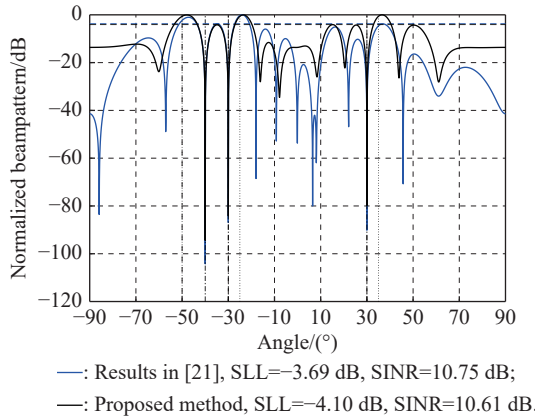

Fig. 6 Comparison of beam patterns simulated with the method in [21] and the proposed method for multiple desired signals

Table 2 Comparison for the level of multiple expected signals with the method in [21] and the proposed method

dB

Method	Expected signal's levels			Average error
	$\theta_{s_1}=-50°$	$\theta_{s_2}=-25°$	$\theta_{s_3}=35°$	
Results in [21]	−2.34	−0.31	−4.61	−2.42
Proposed method	−0.63	−0.63	−0.63	−0.63

The computational time of different methods is compared to illustrate the complexity of the proposed algorithm in Table 3. It is clear that the time spent by the proposed algorithm is almost the same as that of other methods in the case of a single expected signal. However, when there are multiple expected signals in space, the proposed algorithm takes more time than other methods.

Table 3 Computational time of two algorithms

s

Simulation	Method	Computational time
1	DIRR	0.96
	Proposed method	1.97
2	DIRR	1.40
	Proposed method (δ= −10 dB)	18.01
	Proposed method (δ= −20 dB)	24.86
3	Results in [23]	45.65
	Proposed method	47.41
4	Results in [21]	17.55
	Proposed method	69.79

The particular reason for the circumstance is that the branch-and-bound algorithm is employed to solve the array synthesis problem. A branch-and-bound algorithm is usually based on an enumeration process, and the proposed convex programming problem and its convex relaxation form need to be solved alternately to obtain upper and lower bounds, which makes it consume more time. However, the branch operation and the upper and lower bounds in the proposed algorithm can avoid unnecessary branches and improve the problem's computational efficiency compared with the enumeration method [26]. That actively demonstrates that the proposed algorithm improves beamforming performance by sacrificing computational time.

4. Conclusions

In this paper, an effective array adaptive beamforming scheme based on the branch-and-bound algorithm is proposed. Firstly, excellent beamforming performance is realized by adding sidelobe constraints in the Capon algorithm, and the array response phase of the desired signal is optimized by using auxiliary variables. Secondly, the modified reweighted l_1-norm is used to design the sparse array. The whole beamforming is expressed as a convex optimization problem solved with the branch-and-bound scheme. Numerical examples have verified the proposed method exhibits a lower SLL, higher SINR, and less pointing error for both a single expected signal and multiple desired signals of the full array and sparse array. How to achieve superior beamforming performance without sacrificing computation time will be the potential for further work.

References

[1] LIU S, ZHANG X, YAN F G, et al. Fast and accurate covariance matrix reconstruction for adaptive beamforming using Gauss-Legendre quadrature. Journal of Systems Engineering and Electronics, 2021, 32(1): 38–43.

[2] APPLEBAUM S. Adaptive arrays. IEEE Trans. on Antennas and Propagation, 1976, 24(5): 585–598.

[3] FANTE R L, VACCARO J J. Wideband cancellation of interference in a GPS receive array. IEEE Trans. on Aerospace & Electronic Systems, 2000, 36(2): 549–564.

[4] VAN A J, LESHEM A, BOONSTRA A J. Signal processing for radio astronomical arrays. Proc. of the IEEE Sensor Array and Multichannel Signal Processing Workshop, 2004. DOI: 10.1109/SAM.2004.1502901.

[5] MELVIN W L. A STAP overview. IEEE Aerospace and Electronic Systems Magazine, 2004, 19(1): 19–35.

[6] CHEN T, YANG P, PENG H G, et al. Multi-target tracking algorithm based on PHD filter against multi-range-false-target jamming. Journal of Systems Engineering and Electronics, 2020, 31(5): 859–870.

[7] CAPON J. High-resolution frequency-wavenumber spectrum analysis. Proceedings of the IEEE, 1969, 57(8): 1408–1418.

[8] GOU X M, XU Y G, LIU Z W, et al. Capon beamformer for acoustic vector sensor arrays using biquaternions. Proc. of the International Conference on Awareness Science and Technology, 2011: 28–31.

[9] ZHU Y F, ZHAO X Q. One robust capon beamformer for ultrasound imaging. Proc. of the International Conference on Biomedical Engineering and Informatics, 2014: 368–372.

[10] LEBRET H, BOYD S. Antenna array pattern synthesis via convex optimization. IEEE Trans. on Signal Processing, 1997, 45(3): 526–532.

[11] KAJENSKI P J. Phase only antenna pattern notching via a semidefinite programming relaxation. IEEE Trans. on Antennas and Propagation, 2012, 60(5): 2562–2565.

[12] FUCHS B, SKRIVERVIK A, MOSIG J R. Shaped beam synthesis of arrays via sequential convex optimizations. IEEE Antennas and Wireless Propagation Letters, 2013, 12: 1049–1052.

[13] FUCHS B. Array synthesis problems via convex relaxation. Proc. of the IEEE Antennas and Propagation Society International Symposium, 2014: 1361–1362.

[14] FUCHS B. Application of convex relaxation to array synthesis problems. IEEE Trans. on Antennas and Propagation, 2014, 62(2): 634–640.

[15] DEDEOGLU M, ALP Y K, ARIKAN O. FIR filter design by convex optimization using directed iterative rank refinement algorithm. IEEE Trans. on Signal Processing, 2016, 64(9): 2209–2219.

[16] ZHAO Z H, ZHAO H L, ZHENG M G, et al. Real-time phase-only nulling based on deep neural network with robustness. IEEE Access, 2019, 7: 142287–142294.

[17] WANG X, ABOUTANIOS E, TRINKLE M, et al. Reconfigurable adaptive array beamforming by antenna selection. IEEE Trans. on Signal Processing, 2014, 62(9): 2385–2396.

[18] MEHANNA O, SIDIROPOULOS N D, GIANNAKIS G B. Joint multicast beamforming and antenna selection. IEEE Trans. on Signal Processing, 2013, 61(10): 2660–2674.

[19] SIDIROPOULOS N D, DAVIDSON T N, LUO Z Q. Transmit beamforming for physical-layer multicasting. IEEE Trans. on Signal Processing, 2006, 54(6): 2239–2251.

[20] ROY V, CHEPURI S P, LEUS G. Sparsity-enforcing sensor selection for DOA estimation. Proc. of the IEEE International Workshop on Computational Advances in Multi-Sensor Adaptive Processing, 2013: 340–343.

[21] HAMZA S A, AMIN M G, FABRIZIO G. Optimum sparse array beamforming for general rank signal models. Proc. of the IEEE Radar Conference, 2018: 1343–1347.

[22] HAMZA S A, AMIN M G. Hybrid sparse array beamforming design for general rank signal models. IEEE Trans. on Signal Processing, 2019, 67(24): 6215–6226.

[23] ZHENG Z, FU Y P, WANG W Q, et al. Sparse array design for adaptive beamforming via semidefinite relaxation. IEEE Signal Processing Letters, 2020, 27: 925–929.

[24] LU C, LIU Y F, ZHOU J. An efficient global algorithm for nonconvex complex quadratic problems with applications in wireless communications. Proc. of the IEEE/CIC International Conference on Communications in China, 2017: 925–929.

[25] LU C, DENG Z B, ZHANG W Q, et al. Argument division based branch-and-bound algorithm for unit-modulus constrained complex quadratic programming. Journal of Global Optimization, 2018, 70: 171–187.

[26] LU C, LIU Y F, ZHOU J. An enhanced SDR based global algorithm for nonconvex complex quadratic programs with

signal processing applications. IEEE Open Journal of Signal Processing, 2020, 1: 120–134.

Biographies

YE Xiaodong was born in 1967. He received his B.S., M.S., and Ph.D. degrees from Nanjing University of Posts and Telecommunications in 1990, Nanjing Institute of Electric Technology in 1993, and Nanjing University of Aeronautics and Astronautics in 1997, respectively. He was a postdoctor in Nanjing University of Science and Technology (NJUST) from 1997 to 1999. He has been an associate professor in NJUST since 1999. His current research interests involve radar data analysis, modern signal processing, and artificial intelligence technique.
E-mail: yexiaodong@njust.edu.cn

LI Li was born in 1996. She received her B.S. degree in electronic information engineering from Henan Polytechnic University, Henan, China, in 2019. She is currently pursuing her M.S. degree in electronics and communication engineering with Nanjing University of Science and Technology, Nanjing, China. Her current research interests include signal processing and convex optimization.
E-mail: Lily1111@njust.edu.cn

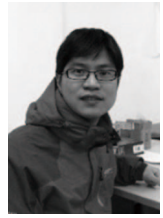

WANG Hao was born in 1980. He received his B.S. and Ph.D. degrees in electrical engineering from Nanjing University of Science and Technology, Nanjing, China, in 2002 and 2009, respectively. He is currently an associate professor with the School of Electronic and Optical Engineering, Nanjing University of Science and Technology. His current research interests include microstrip antennas for wireless communications and terminal antenna subsystem for compass navigation satellite system.
E-mail: haowang@mail.njust.edu.cn

TAO Shifei was born in 1987. He received his B.S. and Ph.D. degrees from the Department of Communication Engineering, Nanjing University of Science and Technology (NJUST), Nanjing, China, in 2008 and 2014, respectively. Since 2017, he has been with NJUST, and now he is an associate professor in the Department of Communication Engineering, NJUST. From 2015 to 2016, he was a postdoctoral research associate in the Department of Electronic and Computer Engineering, Northeastern University, Boston, USA. His current research interests are electromagnetic theory and antenna technology, and SAR images processing.
E-mail: s.tao@njust.edu.cn